Article

Not peer-reviewed version

Regulation of Bimetallic Coordination Centers in MOF Catalyst for Electrochemical CO2 Reduction to Formate

Rui Yang , Qun Huang , Xuelan Sha , Beibei Gao , Juan Peng *

Posted Date: 22 August 2023

doi: 10.20944/preprints202308.1595.v1

Keywords: electrocatalysis; carbon dioxide; formic acid; coordination centers; bimetallic

Article

Regulation of Bimetallic Coordination Centers in MOF Catalyst for Electrochemical CO_2 Reduction to Formate

Rui Yang †, Qun Hang †, Xuelan Sha, Beibei Gao and Juan Peng *

State Key Laboratory of High-Efficiency Utilization of Coal and Green Chemical Engineering, College of Chemistry and Chemical Engineering, Ningxia University, Yinchuan 750021, China; 18709609803@163.com (R.Y.); 18709506169@163.com(Q.H.); shaxuelan2023@163.com (X.S.); gbb214428@163.com (B.G.)

* Correspondence: pengjuan@nxu.edu.cn

† These authors contributed equally to this work.

Abstract: Electrocatalytic reduction of CO_2 to valuable chemicals can alleviate the energy crisis, and solve the greenhouse effect. The key is to develop non-noble metal electrocatalysts with high activity, selectivity and stability. Herein, bimetallic MOF materials (BiZn-MOF, BiSn-MOF and BiIn-MOF) were constructed by coordinating the P-zone transition metals Zn, In, Sn and Bi with the organic ligand 3-amino-1H-1,2,4-triazole-5-carboxylic acid (H_2atzc) through a rapid microwave synthesis approach. The coordination centers in bimetallic MOF Catalyst were regulated to optimize the catalytic performance to CO_2RR. The optimized catalyst BiZn-MOF exhibited high catalytic activity than those of Bi-MOF, BiSn-MOF and BiIn-MOF. The BiZn-MOF exhibited a higher selectivity for formate production with a Faradic efficiency (FE=92%) at a potential of -0.9 V (vs. RHE) with a current density of 13 mA/cm^2. The current density maintained for 13 h continuous electrolysis. The electrochemical conversion of CO_2 to formic acid mainly follows the *OCHO pathway. The good catalytic performance of BiZn-MOF may be attributed to the Bi-Zn bimetallic coordination centers in the MOF, which can reduce the binding energies of the reaction intermediates by tuning the electronic structure and atomic arrangement. This study provides a feasible strategy for performance optimization of bismuth-based catalysts.

Keywords: electrocatalysis; carbon dioxide; formic acid; coordination centers; bimetallic

1. Introduction

The excessive emission of CO_2 is the main cause of the greenhouse effect, which poses a serious threat to global ecology. Converting excessive CO_2 emissions into valuable chemicals and fuels is an effective means of solving both environmental and energy crises [1]. One of the most attractive methods is electrochemical CO_2 reduction reaction (CO_2RR), which uses renewable electricity to convert CO_2 into commercially valuable chemicals and fuels [2]. Formate (Formic acid) is considered a promising product with greater economic feasibility and industrial prospects among many CO_2 reduction products [3]. However, electrochemical CO_2RR still faces great challenges due to limitations in catalyst selection, such as low current density, high overpotential, poor selectivity and stability.

P-zone transition elements such as Sn, Bi, Pb and In exhibit high selectivity for formic acid production during the electrochemical reduction of CO_2 [4–8]. Due to its low cost and effective inhibition of hydrogen evolution reaction (HER), bismuth-based catalysts have become highlight of attention. Building dual or multi-component catalysts can effectively enhance CO_2RR by exerting the synergistic effect of each component [9]. In particular, bimetallic catalysts can enhance the selectivity and activity of CO_2RR by stabilizing the intermediates and inhibiting HER through synergistic effects [10]. Compared with single-metal catalysts, the advantage of bimetallics is that the binding energy of the reaction intermediates can be adjusted by changing the electronic structure and atomic

arrangement [11]. Hence, the researchers focus on combining other metals with Bi to obtain bimetallic electrocatalysts with high selectivity, stability and low overpotential, such as Bi−Sn, Bi−Cu, Bi−Ce, Bi−In and Bi-Zn [12–16]. The bimetallic catalysts showed good catalytic activity and selectivity in the electrochemical CO_2RR process for formic acid preparation. For instance, the strong binding energy between In and *OCHO compensates for the weak binding energy of Bi and *OCHO, which contributes to enhancing the selectivity of formic acid production [17].

Metal organic frameworks (MOFs) have a unique framework structure, which are constructed from various organic ligands and inorganic metal clusters. The controllable properties and structure of MOFs make them ideal materials for catalyst optimization [18–20]. The porosity of MOFs promotes the transport of reactants to active sites [21]. The large specific surface area of MOFs also provides a large number of catalytic active sites, making them suitable for the preparation of electrocatalysts. The metal active sites in MOFs can exist in inorganic nodes or be embedded in the structure of the original MOF. Usually, the synthesized modified cations and different coordination centers that provide different coordination environments. Their chemical environment exhibits excellent properties in coordination, which helps to gain a deeper understanding of how active sites affect their catalytic properties. In addition, the chemical environment can be further adjusted by selecting different types of metal centers [22]. Compared to monometallic MOFs, bimetallic MOFs can adjust the binding energies of the reaction intermediates by tuning the electronic structure and atomic arrangement [23,24]. However, there has been little research on combining the two into one entity due to the inherent low current density problems.

Herein, the P-zone transition metals Zn, In, Sn and Bi were coordinated with the organic ligand 3-amino-1H-1,2,4-triazole-5-carboxylic acid (H_2atzc) through rapid microwave synthesis approach to construct bimetallic MOF materials (BiZn-MOF, BiSn-MOF and BiIn-MOF). The bimetallic coordination centers in MOF catalyst were regulated to optimize the catalytic performance to CO_2RR. The optimized BiZn-MOF exhibited high catalytic activity than those of Bi-MOF, BiSn-MOF and BiIn-MOF. The BiZn-MOF exhibited a higher selectivity for formate production with a faradic efficiency (FE=92%) at a potential of -0.9 V (vs. RHE). The reaction intermediates were monitored by in situ Fourier transform infrared spectroscopy (FT-IR). The results indicated that the electrochemical conversion of CO_2 to formate mainly follows the *OCHO pathway. This work offers an effective way for electroreduction of CO_2 to formate and provides design ideas for constructing other efficient catalysts.

2. Results and Discussion

2.1. Morphology and Structure of Bimetallic MOF

Figure 1a shows the synthesis procedure of BiZn-MOF. The synthesis routes of BiIn-MOF and BiSn-MOF are similar to that of BiZn-MOF. By using 3-amino-1H-1,2,4-triazole-5-carboxylic acid hydrate (H_2atzc) as an organic ligand, the catalysts BiZn-MOF, BiIn-MOF and BiSn-MOF were successfully prepared through a rapid microwave approach. To verify the coordination environments of BiZn-MOF, BiIn-MOF and BiSn-MOF catalysts, Fourier transform infrared spectroscopy (FT-IR) was performed, as shown in Figure 1b. The infrared absorption bands in the range of 3400 cm^{-1} to 3500 cm^{-1} for BiZn-MOF, BiIn-MOF and BiSn-MOF catalysts can be attributed to O-H absorption bands in water molecules. H_2atzc exhibits a stretching vibration at 1690 cm^{-1} due to C=O in the carboxyl group, and a plane stretching vibration mode at 3200 cm^{-1} due to N-H in the amino group. It is worth noting that the characteristic peaks at 1690 cm^{-1} and 3200 cm^{-1} were not appeared in BiZn-MOF, BiIn-MOF and BiSn-MOF catalysts. Therefore, the carboxyl and amino functional groups of the organic ligand H_2atzc successfully coordinated with the metal centers. XRD patterns were conducted to further investigate the phase structure of BiZn-MOF, BiIn-MOF, BiSn-MOF and Bi-MOF catalysts. Figure 1c shows that the diffraction peaks of all four catalysts match their respective characteristic peaks. The pattern of BiZn-MOF corresponded to the characteristic peaks of standard cards (PDF#27-0050) and (PDF#36-1451), respectively. The characteristic peaks at 27.95°, 42.05°, 48.44° and 77.99° correspond to the (201), (320), (410) and (620) crystal faces of Bi_2O_3,

Preprints (www.preprints.org) | NOT PEER-REVIEWED | Posted: 22 August 2023 doi:10.20944/preprints202308.1595.v1

respectively. The characteristic peaks at 31.76°, 34.42°, 47.53°, 56.60° and 66.38° correspond to the (100), (002), (102), (110) and (200) crystal faces of ZnO, respectively. These results suggested that some oxides were formed on the MOF surface. Combination of XRD and FTIR indicated the successful preparation of BiZn-MOF, BiIn-MOF and BiSn-MOF catalysts.

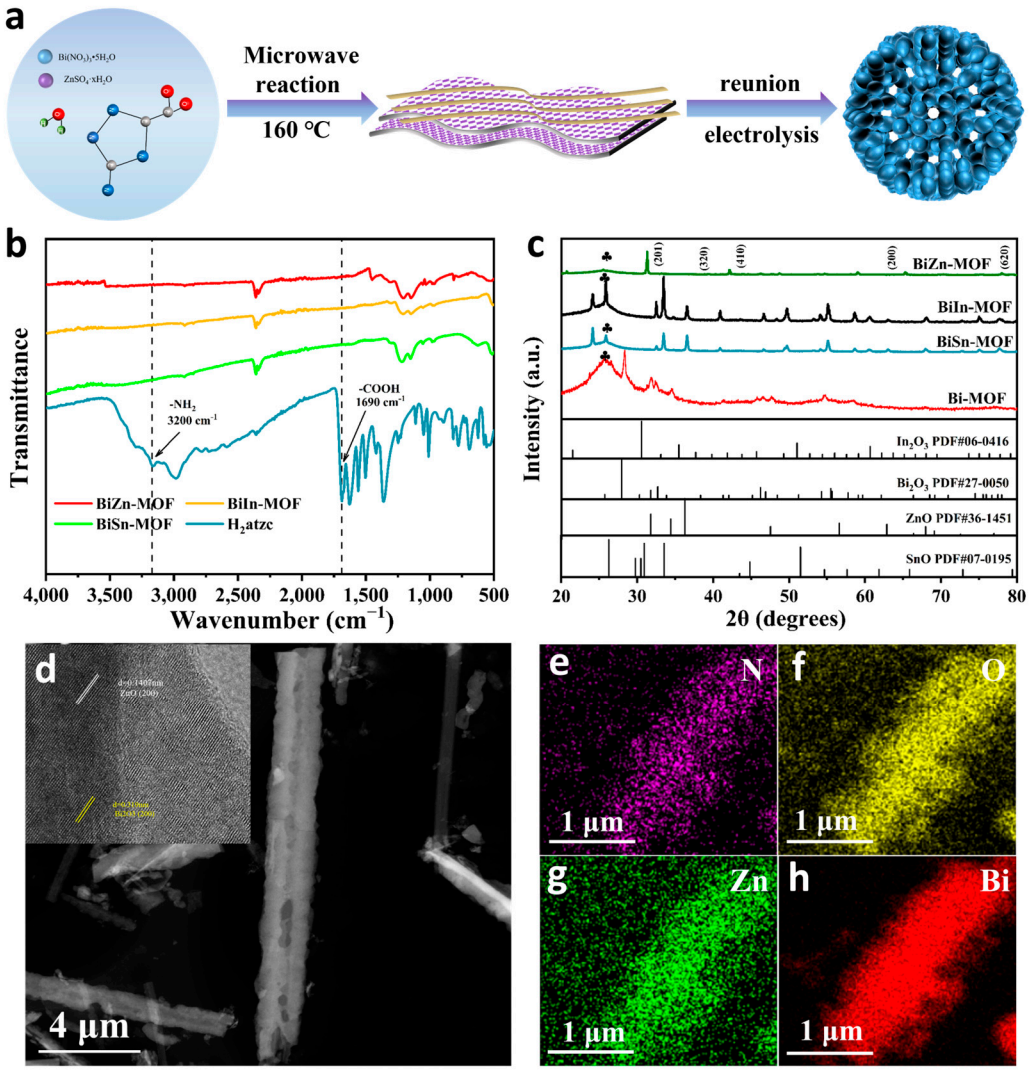

Figure 1. (**a**) Scheme illustration of the synthetic route for BiZn-MOF. (**b**) FT-IR spectra. (c) XRD patterns. (**d**) TEM and HRTEM images of BiZn-MOF. (**e**–**h**) Elemental mapping image (purple, yellow, green and red represent N, O, Zn, Bi, respectively).

Figure S1a–d showed the scanning electron microscope (SEM) images of the catalysts Bi-MOF, BiZn-MOF, BiIn-MOF and BiSn-MOF, respectively. The catalyst Bi-MOF has a spindle-like structure, but the bimetallic MOF showed a different morphology due to the incorporation of different metal ions Zn^{2+}, Sn^{4+} and In^{3+}. From SEM images, the catalyst BiZn-MOF presented a nanorod mophology, which were nano-assemblies formed by the accumulation of nanosheets and nanowires. The catalyst BiIn-MOF is an irregular nanosheet. The catalyst BiSn-MOF has a thick flaky nanoflower structure. Brunner-Emmet-Teller (BET) technique was used to measure the specific surface area of Bi-BTC catalyst, as shown in Figure S2. There are a large number of pores on the surface of nano-rod-like BiZn-MOF catalyst and the pore volume is 0.231cm^3/g. The catalyst has a specific surface area of 8.717 m^2/g, which provides more active sites for the reaction interface. The unique structure and large specific surface area of BiZn-MOF provide a theoretical basis for the excellent electrocatalytic performance in subsequent electrochemical CO_2RR.

Preprints (www.preprints.org) | NOT PEER-REVIEWED | Posted: 22 August 2023 doi:10.20944/preprints202308.1595.v1

transmission electron microscopy (TEM) was used for to further determine the morphology and composition of the catalysts. Figure 1d revealed that the morphology of BiZn-MOF were nanorods. The top right diagram in Figure 1d shows obvious lattice streaks of ZnO and Bi_2O_3 in high resolution transmission electron microscope (HRTEM), with lattice spacing of 0.141 nm and 0.319 nm corresponding to the (200) crystal face of ZnO and the (201) crystal face of Bi_2O_3, respectively. The scanning map of element distribution in Figure 1e–h confirmed that the morphology of BiZn-MOF is a nano-composite formed by the accumulation of nanosheetsand nanowires. All elements evenly distributed, which proves the successful preparation and synthesis of BiZn-MOF. Energy dispersive X-ray spectrum (EDX, Figure S3) verifies the existence of Bi and Zn elements and uniform distribution on the catalyst BiZn-MOF. The atomic content of Bi and Zn was 33% and 0.03%, respectively.

The chemical composition and valence state of the BiZn-MOF catalyst were analyzed by XPS. The obtained XPS spectra were calibrated by aligning the position of peak C(sp2) in the C 1s spectrum with its reference value of 284.4 eV. Figure 2a shows the full XPS spectra of BiZn-MOF, which consists of elements Bi, Zn, C, O and N. In Figure 2b, the sub-peaks at 165 eV and 159 eV in the Bi 4f spectrogram indicate the presence of metal ion Bi^{3+}. The weak peaks at 1045 and 1028 eV in Figure 2c correspond to the Zn 2p in the catalyst. The N 1s spectrum at 406 eV demonstrated the existing of N-H bonding in the MOF catalyst.

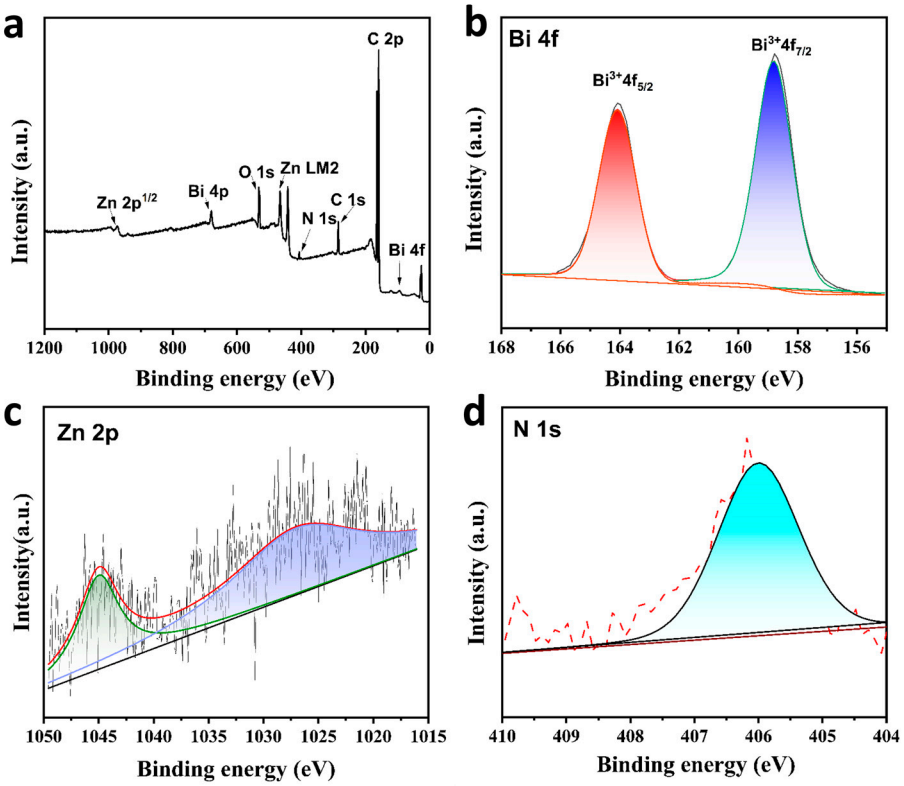

Figure 2. (**a**) XPS survey spectra of BiZn-MOF, (**b**) Bi 4f spectrum of BiZn-MOF, (**c**) Zn 2p spectrum of BiZn-MOF and (**d**) N 1s spectrum of BiZn-MOF.

2.2. Electrocatalytic Performance of CO_2RR

To evaluate the electrochemical properties of BiZn-MOF, BiIn-MOF, BiSn-MOF and Bi-MOF catalysts, linear sweep voltammetry (LSV) curves were first tested using a H-type cell in an electrolyte saturated with CO_2 or N_2. As shown in Figure 3a, **t**he current density of BiZn-MOF to CO_2RR in a saturated CO_2 electrolyte is obviously higher than that in a saturated N_2 electrolyte. This result indicating that the catalyst BiZn-MOF exhibits good electrochemical CO_2RR performance and can significantly suppress the generation of by-products (H_2 and CO). The electrochemical CO_2RR current density of BiZn-MOF is higher than that of BiIn-MOF, BiSn-MOF and Bi-MOF, indicating better catalytic activity for BiZn-MOF compared to those for BiIn-MOF, BiSn-MOF and Bi-MOF, as shown

Preprints (www.preprints.org) | NOT PEER-REVIEWED | Posted: 22 August 2023 doi:10.20944/preprints202308.1595.v1

in Figure 3b. From Figure 3c, the catalyst BiZn-MOF has higher current density and corrected initial potential than BiIn-MOF, BiSn-MOF and Bi-MOF catalysts, indicating its superior electrocatalytic performance for CO_2RR. Figure 3d illustrates the faraday efficiency ($FE_{formate}$) of formate products by four catalysts. The BiZn-MOF exhibits the best catalytic performance among two-component catalysts. At a potential of -0.9 V (vs. RHE), the $FE_{formate}$ reached 92%, which was superior to Bi-MOF (with an $FE_{formate}$ of 78%). This indicates that successful coordination of dual metal center enhances formate selectivity, and BiZn-MOF exerts a bimetallic synergistic effect. Compared with the single component Bi-MOF, BiZn-MOF improves the selectivity of electrocatalytic CO_2 and promotes the formation of formate. Figure 4a–d present a "volcano" diagram showing the selectivity of electrochemical CO_2RR for various products (HCOOH, CO, and H_2) prepared by four catalysts at different potentials. The peak values of BiZn-MOF, BiIn-MOF, BiSn-MOF and Bi-MOF formate are 92%, 78%, 79.5% and 82%, respectively. BiZn-MOF exhibits the highest selectivity for formate.

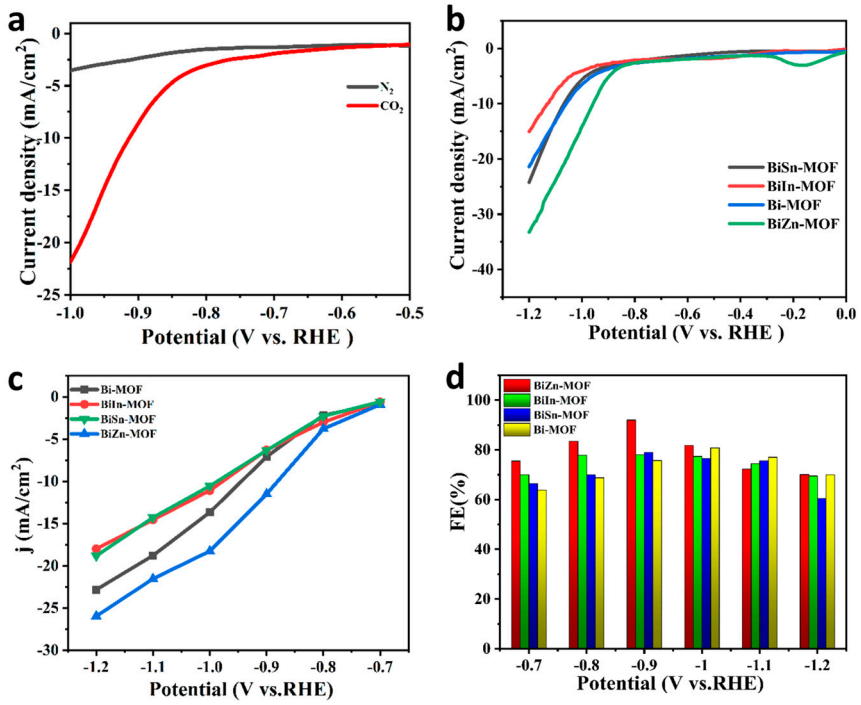

Figure 3. (**a**) Polarization curves of BiZn-MOF in saturated CO_2 and N_2 atmospheres, respectively; (**b**) Polarization curves of BiZn-MOF, BiIn-MOF, BiSn-MOF and Bi-MOF catalysts in saturated CO_2 electrolyte; (**c**) Local current densities (**d**) Faraday efficiency of formate.

To further investigate the effect of electrochemical active surface area (ECSA), cyclic voltammetry (CV) curves were obtained for four catalysts (Bi-MOF, BiZn-MOF, BiIn-MOF and BiSn-MOF) at different sweep speeds (20 -120 mV s^{-1}), as shown in Figure S4a–d. The linear curve was plotted with sweep speed on the horizontal axis and current density difference on the vertical axis. The slope C_{dl} of the linear regression line reflects the magnitude of ECSA. Figure S4e shows that the C_{dl} (180 μF/cm^2) of BiZn-MOF in the two-component catalyst is similar to that of Bi-MOF (150 μF/cm^2). This result confirmed that the differences in CO_2RR performance among the four catalysts mainly depend on the bimetallic centers optimizing, not the ECSA. Electrochemical impedance spectroscopy (EIS) was used to study electrode reaction kinetics at the interface between the electrode and electrolyte. From the EIS in Figure S5a, the semi-circle radius of BiZn-MOF in the two-component catalyst is the smallest (6 Ω), smaller than that of Bi-MOF (27 Ω), BiIn-MOF (9 Ω) and BiSn-MOF (8 Ω). This reflects that with the insertion of Zn^{2+}, the charge transfer rate of BiZn-MOF is accelerated, thus boosting the catalytic activity to CO_2RR. To better understand the reaction kinetics of BiZn-MOF, BiSn-MOF and BiIn-MOF catalysts, Tafel slope analysis was performed. As shown in Figure S5b, the Tafel slopes of BiZn-MOF (106 mV dec^{-1}) and BiIn-MOF (104 mV dec^{-1}) are lower than that of BiSn-

Preprints (www.preprints.org) | NOT PEER-REVIEWED | Posted: 22 August 2023 doi:10.20944/preprints202308.1595.v1

MOF (140 mV dec^{-1}). These results indicate that the electron transfer rate of BiZn-MOF and BiIn-MOF catalysts is fast, which is conducive to the adsorption and desorption of *CO on their surfaces.

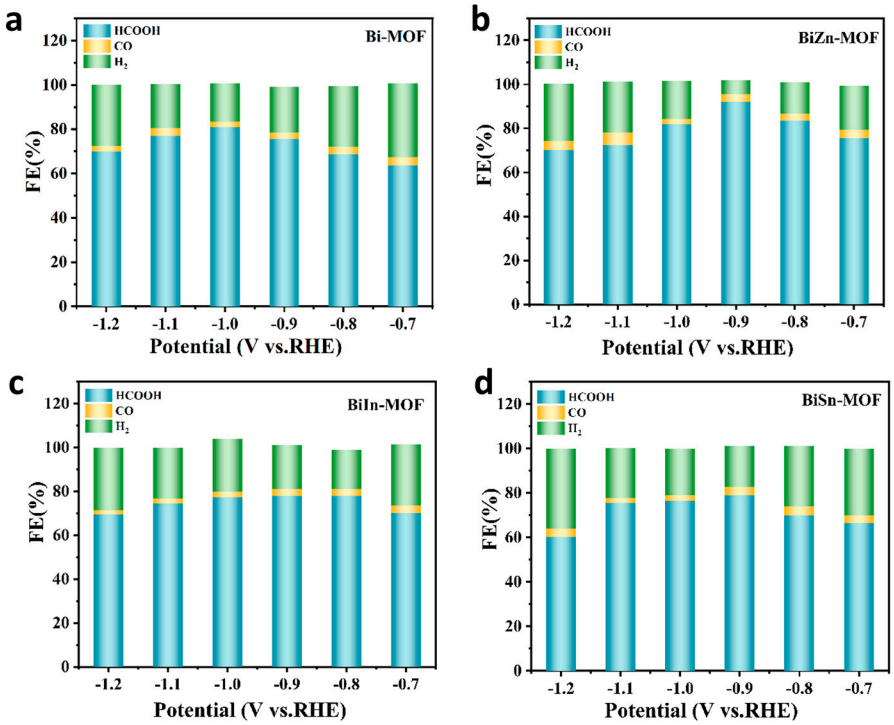

Figure 4. FEs of $HCOO^-$, H_2 and CO: (**a**) Bi-MOF, (**b**) BiZn-MOF, (**c**) BiIn-MOF and (**d**) BiSn-MOF.

Figure S6a–c displays the constant potential electrolysis of CO_2 at various potentials. The stable current density indicates that BiZn-MOF, BiIn-MOF, and BiSn-MOF catalysts exhibit good electrochemical stability in the CO_2RR. By further exploring the stability of CO_2RR materials, BiZn-MOF decomposes for about 13 hours at a potential of -0.9 V (vs. RHE) in Figure S6d. The current density of BiZn-MOF remains stable at 13 mA/cm^2, and the Faraday efficiency of producing formate products by electrochemical CO_2RR is approximately 92%. These results indicate that BiZn-MOF exhibits good stability towards CO_2RR.

Powder X-ray diffraction (XRD) was used to further confirm the phase purity and composition of BiZn-MOF catalyst after electrolysis, as shown in Figure 5a. It was observed that new characteristic diffraction peaks appeared after CO_2 electrolysis. By comparing the standard cards (PDF#04-0831) and (PDF#41-1449), diffraction peaks at 36.29°, 38.99°, 43.23°, 54.33°, 70.66° and 77.02° corresponded to crystal faces (002), (100), (101), (102), (110) and (004) of Zn, respectively. The angles of 26.92° and 32.48°corresponded to Bi_2O_3's crystal faces of (111) and (-211). This is because that some Zn^{2+} was reduced to Zn after the electrolysis of the catalyst BiZn-MOF. The SEM image in Figure 5b revealed that agglomeration occurred on the surface of BiZn-MOF after electrolysis, mainly due to structural changes caused by partial reduction of Zn^{2+}. Figure 5c shows a survey XPS spectra, indicating that BiZn-MOF still contains elements Bi, Zn, C, N and O after electrolysis. The XPS spectrum of Bi 4f in Figure 5d revealed the presence of metal ion Bi^{3+} at peaks of 165 eV and 159 eV, which was consistent with the results from XRD pattern. In Figure S5c, Zn 2p spectrum showed that the binding energy at 1021 eV corresponds to the diffraction peak of Zn (0), and the peak signal changed, mainly due to the low content of Zn in BiZn-MOF catalyst and partial shedding (wt=0.02%) after electrolysis. In Figure S5d, N 1s spectra showed the same coordination pattern as that of pre-electrolysis catalyst BiZn-MOF. In Figure S7a, energy dispersive X-ray spectrometer (EDX) showed that Bi and Zn elements were evenly distributed on the catalyst BiZn-MOF after electrolysis, which verified the presence of Zn elements post-electrolysis. The content of Bi and Zn is 69.66% and 0.02%, respectively, indicating that some Zn may have been lost during the electrolysis process of BiZn-MOF, resulting in a decrease in its content. The element distribution mapping further confirmed that agglomeration occurred on the

Preprints (www.preprints.org) | NOT PEER-REVIEWED | Posted: 22 August 2023 doi:10.20944/preprints202308.1595.v1

surface of BiZn-MOF catalyst after electrolysis, while the elements C (blue), N (purple), O (yellow), Bi (red) and Zn (green) were uniformly distributed.

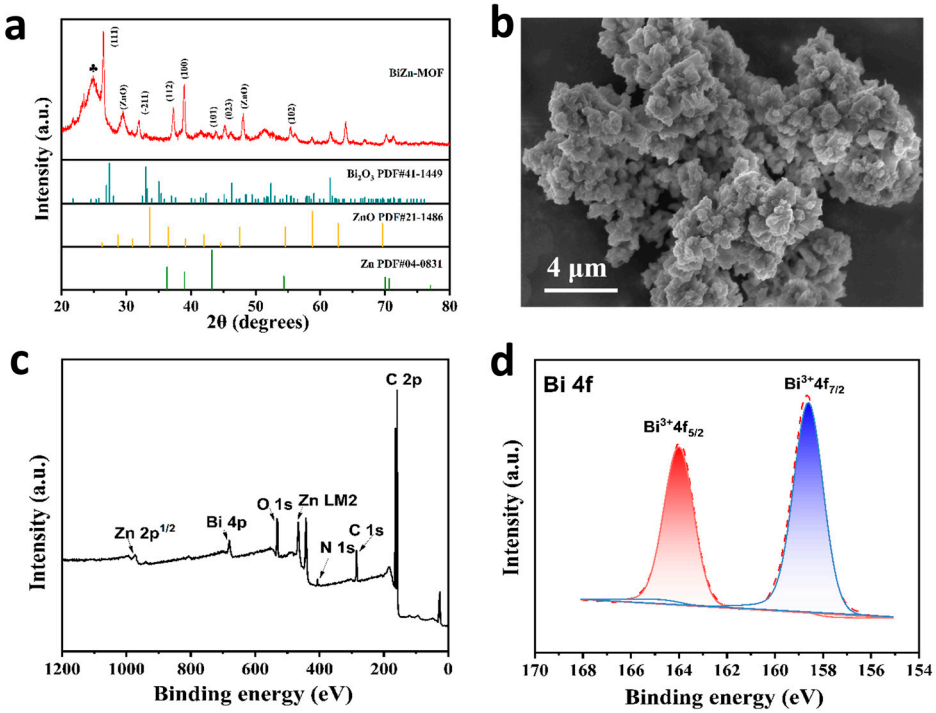

Figure 5. Characterizations of BiZn-MOF catalyst after electrolysis for 10 h. (**a**) XRD pattern. (**b**) SEM image. (**c**) XPS spectra. (**d**) Bi 4f XPS spectra.

Electrochemical CO_2RR is a promising electrocatalytic technology, but due to the slow kinetics of oxygen evolution (OER) at the anode during electrolysis, a large amount of energy is needed. BiZn-MOF exhibited excellent electrocatalytic activity and selectivity in the process of electrocatalytic CO_2 reduction. To confirm the practical application the BiZn-MOF catalyst, an whole electrolytic cell was assembled by coupling the cathode material BiZn-MOF with the anode material IrO_2. Figure 6a shows that a current density of 9 mA/cm^2 can be achieved with a cell voltage of 3.5 V and 5 mA/cm^2 at 3.0 V. After constant potential current-time curve (I-t) test on $CO_2RR \| OER$ (Figure 6b), it is found that BiZn-MOF$\|IrO_2$ can maintain stability for up to 10 h at 3.0 V, indicating application prospects for BiZn-MOF$\|IrO_2$, despite the expensive anode material IrO_2, which has good stability and OER catalytic activity.

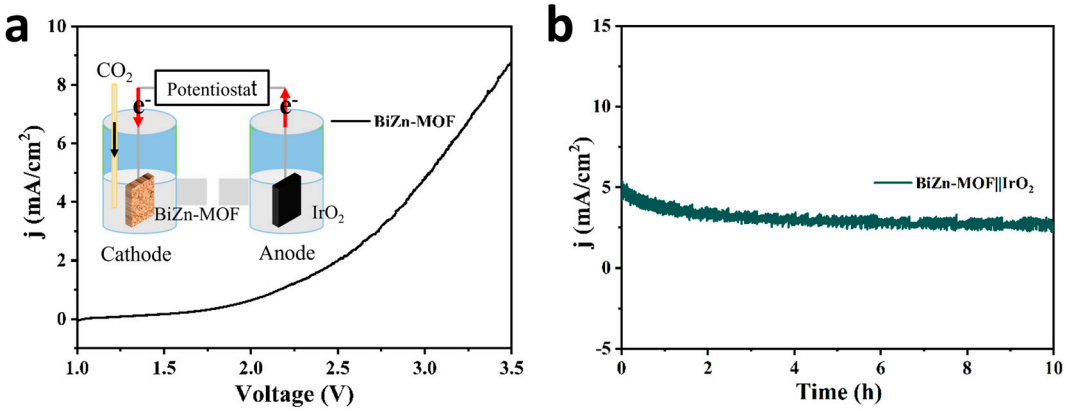

Figure 6. Performance of the $CO_2RR \| OER$ full cell for overall CO_2 splitting: (**a**) LSV curves for the $CO_2RR \| OER$ full cell based on the BiZn-MOF $\| IrO_2$ pair and (**b**) I-t curves at 3.0 V in $CO_2RR \| OER$ full cell.

Preprints (www.preprints.org) | NOT PEER-REVIEWED | Posted: 22 August 2023 doi:10.20944/preprints202308.1595.v1

2.3. Catalytic Mechanism

To better study the reaction pathway and mechanism of electrocatalytic CO_2RR for formate formation by catalyst, in-situ Fourier transform infrared spectroscopy (FT-IR) was used to detect catalytic reaction intermediates. The FT-IR spectra can reflect molecular structure, identify structural composition and determine the presence of chemical groups [25], thus the enabling detection of reaction intermediates. In Figure 7a, FTIR of BiZn-MOF was tested in a CO_2-saturated 0.5 M $KHCO_3$ electrolyte with different potential windows (-1.2V to -1.7 V) for electrolysis. Distinct peaks of $*CO_2$ intermediates are observed within the wavelength range of 1150 cm^{-1} and 1704 cm^{-1}, which play a crucial role in electrocatalytic CO_2 reduction to formate. Additionally, the characteristic absorption peak of CO_3^{2-} is observed at 1450 cm^{-1}, while the stretching vibration of C-O bond in CO_3^{2-} manifests at 1510 cm^{-1} [26]. The symmetrical tensile vibration of OCO in *OCHO intermediates is observed at 1435 cm^{-1}. The vibration pattern of OCO was also observed during the adsorption of *OCHO intermediates and formate. The FTIR in Figure 7b displays a distinctive peak at 1435 cm^{-1}. With intensity gradually increased as electrolysis time extending, indicating an increase in the vibration mode of OCO. This result further clarifies the electrochemical CO_2RR to formate followed the *OCHO reaction pathway.

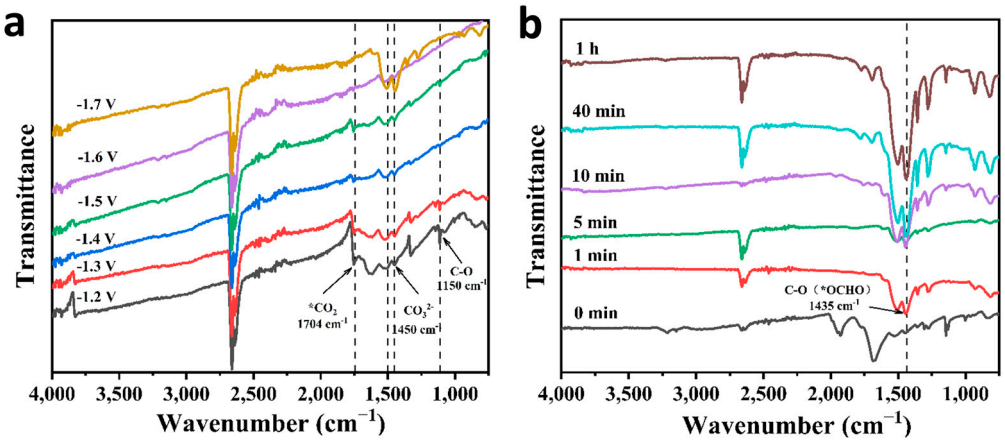

Figure 7. In-situ FTIR of BiZn-MOF **(a)** electrolysis at a potential of -1.2 V to -1.7 V for 1 h, and **(b)** at a potential of -0.9 V (vs. RHE) for different electrolysis times.

When preparing formate (or formic acid) via electrochemical CO_2RR, two reaction pathways exist [27]:

$$CO_2+H^++e^-\rightarrow *OCHO\ (or\ *COOH)+H^++e^-\rightarrow HCOOH$$

The final transformation of the reaction intermediate into either HCOOH or CO is affected by the pH of the electrolyte, which is a key factor in determining the product. Generally speaking, alkaline conditions are more conducive to forming *OCHO intermediates [28–30]. This study employs a 0.5 M $KHCO_3$ solution (pH=8.2) with an alkaline condition, so it is more conducive to *OCHO formation, thus obtainning e^- to generate formate (or formic acid). Simultaneously, *OCHO exhibits enhanced affinity towards the bimetallic active centers Bi and Zn in catalytic material BiZn-MOF, leading to the formation of Bi-O and Zn-O bonds that ensure surface stability [31]. Due to the strong electron-withdrawing ability of *COOH, it favors the formation of Bi-C or Zn-C bonds and C-C coupling [32]. However, in this study, only HCOOH and CO products were detected instead of C2 products, which further supports the proposed *OCHO reaction pathway.

 doi:10.20944/preprints202308.1595.v1

3. Materials and Methods

3.1. Synthesis of Bimetallic MOF Catalysts

Firstly, $ZnSO_4 \cdot xH_2O$ (69.41 mg) and Bi $(NO_3)_3 \cdot 5H_2O$ (340 mg) were dissolved in deionized water (60 mL), and then mixed with H_2atzc (89.7 mg). Subsequently, it was stirred at room temperature for 30 minutes and transferred to a microwave reactor at 160 °C for 1.5 h. Finally, the catalytic materials BiZn-MOF were centrifuged for three times and then put into a drying oven at 60 °C to dry the samples. Other three catalysts (BiIn-MOF, BiSn-MOF and Bi-MOF) were prepared with the similar procedure to the BiZn-MOF by changing the metal sources.

3.2. Electrochemical Measurements

The carbon paper was ultrasonic in acetone and deionized water for 1 h. 5 mg of BiZn-MOF (or BiIn-MOF, BiSn-MOF Bi-MOF) were put into 50 μL Nafion solution, 500 μL deionized water and 450 μL ethanol and ultrasound to prepare the catalyst ink. Finally, a dried carbon paper (1cm×1cm) with a load of 1 mg/cm^2 catalyst was prepared by transferring appropriate ink drops onto the carbon paper.

All electrochemical tests were carried out at room temperature, using a type H cell for this work. The cathode chamber and the anode chamber are separated by a proton exchange membrane. A certain volume of 0.5 M $KHCO_3$ electrolyte was measured in the cathode chamber and the anode chamber. In the preparation stage of the experiment, the inlet flow rate was 20 mL/min and CO_2 gas was ventilated for 40 min until the electrolyte in the cathode chamber reached saturation. A three-electrode system was adopted, with platinum sheet as the counter electrode and Ag/AgCl (saturated KCl) as the reference electrode and the working electrode in the cathode chamber. After that, keep the three electrodes at the same height. All electrochemical tests were performed on the Shanghai Chenhua CHI 760D, where the pH of the CO_2 saturated electrolyte was 6.8. All potentials in this study were measured with respect to Ag/AgCl reference electrodes. The calculation formula is as follows:

$$\mathrm{E（vs.\ RHE）=E(vs.\ Ag/AgCl)} + 0.222\ \mathrm{V} + 0.0591 \times \mathrm{pH}$$

3.3. Product Analysis

The gas phase product was directly detected by gas chromatography (GC7900, Tianmei, China) after coming out of the gas outlet of the H-type electrolytic cell. The carbon-containing gas products in the cathode chamber were analyzed by a methane reformer and a flame ionization detector (FID). A thermal detector (TCD) was used to detect CO_2RR byproduct H_2. Gas products (CO, H_2) are detected when the current tends to be stable. The faraday efficiency of gas products is calculated as follows:

$$\mathrm{FE（H_2/CO）} = \frac{v \times t \times C \times N \times F}{60 \times 24 \times 1000 \times Q} \times 100\% = \frac{v \times C \times 2 \times 96485}{60 \times 24000 \times Q} \times 100\%$$

where ν represents the supplied CO_2 gas flow rate (20 mL/min), C denotes the concentration of H_2 (or CO) in the GC sample ring, *N* is the number of electrons transferred by H_2 or CO molecules (N=2), *F* stands for Faraday efficiency (96485 *C*/mol), and *Q* represents the amount of electrolytic charge.

The liquid products after electrolysis were detected by ion chromatography (AS-DV, Thermo Scientific, New York City, MA, USA). Several quantities of formate products were collected from the cathode chamber in the H-type electrolytic cell and injected into the ion chromatography. The concentration (ppm) of formate in liquid phase products was determined by the integral area of the $HCOO^-$ standard curve. Faraday's formula is as follows:

$$\mathrm{FE_{formate}\ (\%)} = \frac{n_{formate} \times N \times F}{Q} \times 100\% = \frac{C_{formate} \times V \times 2 \times 96485}{I \times t} \times 100\%$$

Where nformate is the molar amount of formate in the cathode chamber, *N* represents the number of electrons required to generate HCOO-, *F* denotes the Faraday constant (96485 C/mol), and *Q* indicates the amount of electron transfer charge (C). For each potential, the liquid phase product in the cathode chamber was collected 3-4 times to obtain an average value. The liquid phase product was then

detected using ion chromatography. The concentration of the liquid phase product was calculated based on the peak area of a standard curve, allowing for determination of the Faraday efficiency of formate production.

4. Conclusions

In summary, bimetallic catalysts BiZn-MOF, BiSn-MOF, and BiIn-MOF were successfully synthesized using a rapid microwave method. The optimized catalysts BiZn-MOF exhibits good catalytic activity for electrochemical CO_2 reduction to formate. At a potential of -0.9 V (vs. RHE), the formate Faradaic efficiency reaches 92%. The good catalytic performance of BiZn-MOF may be attributed to the Bi-Zn bimetallic coordination centers in the MOF, which can reduce the binding energies of the reaction intermediates by tuning the electronic structure and atomic arrangement. This study presents a rational design concept for bimetallic catalysts in CO_2RR research using a facile microwave method.

Supplementary Materials: The following supporting information can be downloaded at: www.mdpi.com/xxx/s.

Author Contributions: Conceptualization, J.P.; methodology, R.Y. and Q.H.; formal analysis, Q.H. and X.S.; investigation, R.Y. and Q.H.; resources, J.P.; data curation, R.Y. and Q.H.; writing-original draft preparation, R.Y., Q.H. and J.P.; writing-review and editing, J.P.; visualization, X.S. and B.G.; project administration, J.P.; funding acquisition, B.G, J.P. All authors have read and agreed to the published version of the manuscript.

Funding: This work was funded by the support from the National Natural Science Foundation of China (No. 22262027). We also acknowledged College Students' Innovative and Entrepreneurship Training Program of Ningxia University (No. G202210749020).

Institutional Review Board Statement: Not applicable.

Informed Consent Statement: Not applicable.

Data Availability Statement: All data in this study can be found in public data bases and Supplementary Information, as described in the Material and Methods section (Section 3).

Conflicts of Interest: The authors declared no competing financial interest.

References

1. Fernández-Torres, M. J.; Dednam, W.; Caballero, J. A. Economic and environmental assessment of directly converting CO_2 into a gasoline fuel. *Energy Conversion and Management.* **2022,** 252, 115115.
2. Ma, W.; He, X.; Wang, W.; Xie, S.; Zhang, Q.; Wang, Y. Electrocatalytic reduction of CO_2 and CO to multi-carbon compounds over Cu-based catalysts. *Chemical Society Reviews.* **2021,** 50, 12897-12914.
3. Kang, D.; Byun, J.; Han, J. Evaluating the environmental impacts of formic acid production from CO_2: catalytic hydrogenation vs. electrocatalytic reduction. *Green Chemistry.* **2021,** 23, 9470-9478.
4. Zhu, C.; Wang, Q.; Wu, C. Rapid and scalable synthesis of bismuth dendrites on copper mesh as a high-performance cathode for electroreduction of CO_2 to formate. *Journal of CO_2 Utilization.* **2020,** 36, 96-104.
5. Li, M.; Wang, H.; Luo, W.; Sherrell, P. C.; Chen, J.; Yang, J. Heterogeneous single-atom catalysts for electrochemical CO_2 reduction reaction. *Advanced Materials.* **2020,** 32, 2001848.
6. Li, J.; Zhu, M.; Han, Y. F. Recent advances in electrochemical CO_2 reduction on indium-based catalysts. *ChemCatChem.* **2021,** 13, 514-531.
7. Yan, L.; Wu, Z.; Li, C.; Wang, J. Sb-doped SnS2 nanosheets enhance electrochemical reduction of carbon dioxide to formate. *Journal of Industrial and Engineering Chemistry.* **2023,** 123, 33-40.
8. Ai, L.; Ng, S.-F.; Ong, W.-J. Carbon dioxide electroreduction into formic acid and ethylene: a review. *Environmental Chemistry Letters.* **2022,** 20, 3555-3612.
9. Pavesi, D.; Ali, F. S.; Anastasiadou, D.; Kallio, T.; Figueiredo, M.; Gruter, G.-J. M.; Koper, M. T.; Schouten, K. J. P. CO_2 electroreduction on bimetallic Pd–In nanoparticles. *Catalysis Science & Technology.* **2020,** 10, 4264-4270.
10. Yang, C.; Hu, Y.; Li, S.; Huang, Q.; Peng, J. Self-Supporting Bi–Sb Bimetallic Nanoleaf for Electrochemical Synthesis of Formate by Highly Selective CO_2 Reduction. *ACS Applied Materials & Interfaces.* **2023,** 15, 6942-6950.
11. Wang, Y.; Cao, L.; Libretto, N. J.; Li, X.; Li, C.; Wan, Y.; He, C.; Lee, J.; Gregg, J.; Zong, H. Ensemble effect in bimetallic electrocatalysts for CO_2 reduction. *Journal of the American Chemical Society.* **2019,** 141, 16635-16642.

12. Han, N.; Ding, P.; He, L.; Li, Y.; Li, Y. Promises of main group metal–based nanostructured materials for electrochemical CO_2 reduction to formate. *Advanced Energy Materials.* **2020,** 10, 1902338.
13. Peng, L.; Wang, Y.; Wang, Y.; Xu, N.; Lou, W.; Liu, P.; Cai, D.; Huang, H.; Qiao, J. Separated growth of Bi-Cu bimetallic electrocatalysts on defective copper foam for highly converting CO_2 to formate with alkaline anion-exchange membrane beyond $KHCO_3$ electrolyte. *Applied Catalysis B: Environmental.* **2021,** 288, 120003.
14. Wang, M.; Liu, S.; Chen, B.; Tian, F.; Peng, C. Synergistic geometric and electronic effects in Bi–Cu bimetallic catalysts for CO_2 electroreduction to formate over a wide potential window. *ACS Sustainable Chemistry & Engineering.* **2022,** 10, 5693-5701.
15. Allioux, F.-M.; Merhebi, S.; Ghasemian, M. B.; Tang, J.; Merenda, A.; Abbasi, R.; Mayyas, M.; Daeneke, T.; O'Mullane, A. P.; Daiyan, R. Bi–Sn catalytic foam governed by nanometallurgy of liquid metals. *Nano letters.* **2020,** 20, 4403-4409.
16. Yao, K.; Wang, H.; Yang, X.; Huang, Y.; Kou, C.; Jing, T.; Chen, S.; Wang, Z.; Liu, Y.; Liang, H. Metal-organic framework derived dual-metal sites for electroreduction of carbon dioxide to HCOOH. *Applied Catalysis B: Environmental.* **2022,** 311, 121377.
17. He, C.; Zhang, Y.; Zhang, Y.; Zhao, L.; Yuan, L. P.; Zhang, J.; Ma, J.; Hu, J. S. Molecular evidence for metallic cobalt boosting CO_2 electroreduction on pyridinic nitrogen. *Angewandte Chemie.* **2020,** 132, 4944-4949.
18. Wang, K.; Li, Y.; Xie, L.-H.; Li, X.; Li, J.-R. Construction and application of base-stable MOFs: a critical review. *Chemical Society Reviews.* **2022,** 51, 6417-6441.
19. Liu, C.; Wang, J.; Wan, J.; Yu, C. MOF-on-MOF hybrids: Synthesis and applications. *Coordination Chemistry Reviews.* **2021,** 432, 213743.
20. Ye, Z.; Jiang, Y.; Li, L.; Wu, F.; Chen, R. Rational design of MOF-based materials for next-generation rechargeable batteries. *Nano-Micro Letters.* **2021,** 13, 1-37.
21. Zhang, X.; Luo, J.; Wan, K.; Plessers, D.; Sels, B.; Song, J.; Chen, L.; Zhang, T.; Tang, P.; Morante, J. R. From rational design of a new bimetallic MOF family with tunable linkers to OER catalysts. *Journal of Materials Chemistry A.* **2019,** 7, 1616-1628.
22. Du, C.; Wang, X.; Chen, W.; Feng, S.; Wen, J.; Wu, Y. CO_2 transformation to multicarbon products by photocatalysis and electrocatalysis. *Materials Today Advances.* **2020,** 6, 100071.
23. Guan, X.; Gao, W.; Jiang, Q. Design of bimetallic atomic catalysts for CO_2 reduction based on an effective descriptor. *Journal of Materials Chemistry A.* **2021,** 9, 4770-4780.
24. Zhong, H.; Ghorbani-Asl, M.; Ly, K. H.; Zhang, J.; Ge, J.; Wang, M.; Liao, Z.; Makarov, D.; Zschech, E.; Brunner, E. Synergistic electroreduction of carbon dioxide to carbon monoxide on bimetallic layered conjugated metal-organic frameworks. *Nature communications.* **2020,** 11, 1409.
25. Zu, X.; Zhao, Y.; Li, X.; Chen, R.; Shao, W.; Wang, Z.; Hu, J.; Zhu, J.; Pan, Y.; Sun, Y. Ultrastable and efficient visible-light-driven CO_2 reduction triggered by regenerative oxygen-vacancies in $Bi_2O_2CO_3$ nanosheets. *Angewandte Chemie International Edition.* **2021,** 60, 13840-13846.
26. Xing, Y.; Kong, X.; Guo, X.; Liu, Y.; Li, Q.; Zhang, Y.; Sheng, Y.; Yang, X.; Geng, Z.; Zeng, J. Bi@ Sn core–shell structure with compressive strain boosts the electroreduction of CO_2 into formic acid. *Advanced Science.* **2020,** 7, 1902989.
27. Yang, W.; Dastafkan, K.; Jia, C.; Zhao, C. Design of electrocatalysts and electrochemical cells for carbon dioxide reduction reactions. *Advanced Materials Technologies.* **2018,** 3, 1700377.
28. Kwon, I. S.; Debela, T. T.; Kwak, I. H.; Seo, H. W.; Park, K.; Kim, D.; Yoo, S. J.; Kim, J.-G.; Park, J.; Kang, H. S. Selective electrochemical reduction of carbon dioxide to formic acid using indium–zinc bimetallic nanocrystals. *Journal of Materials Chemistry A.* **2019,** 7, 22879-22883.
29. Jiang, H.; Zhao, Y.; Wang, L.; Kong, Y.; Li, F.; Li, P. Electrochemical CO_2 reduction to formate on Tin cathode: Influence of anode materials. *Journal of CO_2 Utilization.* **2018,** 26, 408-414.
30. Hai, G.; Xue, X.; Feng, S.; Ma, Y.; Huang, X. High-Throughput Computational Screening of Metal–Organic Frameworks as High-Performance Electrocatalysts for CO_2RR. *ACS Catalysis.* **2022,** 12, 15271-15281.
31. Fernández-Caso, K.; Díaz-Sainz, G.; Alvarez-Guerra, M.; Irabien, A. Electroreduction of CO_2: advances in the continuous production of formic acid and formate. *ACS Energy Letters.* **2023,** 8, 1992-2024.
32. Guo, Z.; Zhang, Q.; Wang, H.; Tan, X.; Shi, F.; Xiong, C.; Man, N.; Hu, H.; Liu, G.; Jiang, J. Bi–Zn codoping in GeTe synergistically enhances band convergence and phonon scattering for high thermoelectric performance. *Journal of Materials Chemistry A.* **2020,** 8, 21642-21648.